

Exploring the initial stages in heavy-ion collisions with high- p_{\perp} R_{AA} and v_2 theory and data

Dusan Zigic¹, Bojana Ilic¹, Marko Djordjevic² and Magdalena Djordjevic¹

¹*Institute of Physics Belgrade, University of Belgrade, Belgrade, Serbia*

²*Faculty of Biology, University of Belgrade, Belgrade, Serbia*

(Dated: September 2, 2019)

Traditionally, low- p_{\perp} sector is used to infer the features of initial stages before QGP thermalization. On the other hand, recently acquired wealth of high- p_{\perp} experimental data paves the way to utilize the high- p_{\perp} particles energy loss in exploring the initial stages. We here study how four different commonly considered initial-stage scenarios which have the same temperature profile after, but differ in the 'temperature' profile before thermalization affect predictions of high- p_{\perp} R_{AA} and v_2 observables. Contrary to common expectations, we obtain that high- p_{\perp} v_2 is insensitive to the initial stages of medium evolution, being unable to discriminate between different conditions. On the other hand, R_{AA} is sensitive to these conditions, however, within the current errorbars, the sensitivity is not sufficient to distinguish between different initial stages. Moreover, we also reconsider the validity of widely-used procedure of fitting the energy loss parameters, individually for different initial-stage cases, to reproduce the experimentally observed R_{AA} . We here find that previously reported sensitivity of v_2 to different initial states is mainly a consequence of the R_{AA} fitting procedure, which may lead to incorrect conclusions. On the other hand, if a global property, in particular the same average temperature, is imposed to tested temperature profiles, high sensitivity of high- p_{\perp} v_2 is again obtained. We however show that this sensitivity would not be a consequence of differences in initial, but rather final, stages. Consequently, the simultaneous study of high- p_{\perp} R_{AA} and v_2 , with consistent energy loss parametrization and stringently controlled temperature profiles, is necessary to assess sensitivity of different variables to differences in initial and final stages.

I. INTRODUCTION

It is by now firmly confirmed that a new state of matter – the quark-gluon plasma (QGP) [1, 2], in which quarks, antiquarks and gluons are deconfined, is formed at the Relativistic Heavy Ion Collider (RHIC) and the Large Hadron Collider (LHC). Rare high transverse momentum (high- p_{\perp}) particles, which are created immediately upon the collision, are sensitive to all stages of QGP evolution, and are considered to be excellent probes [3–6] of this extreme form of matter. As these probes traverse QGP, they lose energy, which is commonly assessed through high- p_{\perp} angular averaged (R_{AA}) [7–14] and high- p_{\perp} angular differential (v_2) [15–19] nuclear modification factors.

Commonly, the high- p_{\perp} particles are used to study the nature of jet-medium interactions, while the low- p_{\perp} particles are used to infer the bulk QGP properties. Accordingly, the scarce knowledge of the features of initial stages before QGP thermalization ($\tau < \tau_0$) was mostly inferred by utilizing data from low- p_{\perp} sector [20–22] ($p_{\perp} \lesssim 5$ GeV). However, since high- p_{\perp} partons effectively probe QGP properties, which in turn depend on initial stages, the idea of utilizing high- p_{\perp} theory and data in exploring the initial stages emerged. This idea acquired an additional boost, since a wealth of precision high- p_{\perp} R_{AA} [7–12] and v_2 [15–19] data have recently become available. Thus, the main goal of this paper is to assess to what extent and through what observables, the initial stages of QGP evolution can be restrained by exploiting the energy loss of high- p_{\perp} particles in evolving medium.

While clarifying these issues is clearly intriguing, the results of current theoretical studies on this subject are either inconclusive or questionable [23–25], as e.g., the energy loss parameters are fitted to reproduce the experimentally observed high- p_{\perp} R_{AA} data, individually for different analyzed initial stages. The energy loss parametrization should, however, clearly be a property of high- p_{\perp} parton interactions with the medium, rather than of individual temperature profiles. Consequently, to more rigorously study this issue, one needs a high control on both the energy loss and the analyzed temperature (T) profiles. To achieve this, we here use our state-of-the-art dynamical energy loss formalism, embedded in Bjorken 1+1D medium evolution [26] (DREENA-B framework [27]). Bjorken 1+1D medium evolution has a major advantage for this study, as it allows to analytically introduce different evolutions before thermalization, with the same evolution after thermalization, which therefore allows to clearly isolate only the effects of different initial stages. Consequently, we will here con-

sider the effects on high- p_{\perp} R_{AA} and v_2 predictions of four common initial-stage cases [23], which have the same T profiles after, but differ in T profiles before the thermalization.

Furthermore, we recently demonstrated that DREENA-B framework is able to accurately reproduce both high- p_{\perp} R_{AA} and v_2 data for diverse colliding systems and energies ($Pb + Pb$ at 2.76 TeV and 5.02 TeV and $Xe + Xe$ at 5.44 TeV), for both light and heavy flavors (h^{\pm} , B, D) and all available centralities, without introducing new phenomena [28, 29]. This is in distinction to many other formalisms, which employ more advanced medium evolution models, but contain simplified energy loss models, which have a tendency to underestimate v_2 relative to the experimental data, which is widely known as the v_2 puzzle [30, 31]. Moreover, we recently obtained that going from 1+1D Bjorken to full 3+1D hydrodynamics evolution [32], does not significantly change the agreement between our predictions and experimental data, strongly suggesting that, for high- p_{\perp} data, accurate energy loss description is more important than the medium evolution. Consequently, for this study, using 1+1D Bjorken evolution has a major advantage of a tight control over the temperature profiles used to mimic different initial states, while, at the same time, providing a reasonably realistic description of the data within our model.

The paper is organized as follows. In Section II, theoretical and computational frameworks are outlined. In Section III, we first assess the sensitivity of R_{AA} and v_2 to the aforementioned initial stages. We then adopt the approach of fitting initial temperature (T_0) to reproduce the same R_{AA} in all cases, and then assess the effect of thus obtained "modified" temperature profiles on R_{AA} and v_2 . We finally reexamine the validity of widely-used procedure [23–25] of fitting the energy loss parameters for different initial-stage cases to reproduce the same R_{AA} . For all these studies, we analytically pinpoint the origin of the obtained results. Our conclusions are presented in Section IV.

II. THEORETICAL AND COMPUTATIONAL FRAMEWORKS

To obtain the medium modified distribution of high- p_{\perp} light and heavy flavor particles, the generic pQCD convolution formula [33, 34] is utilized:

$$\frac{E_f d^3\sigma}{dp_f^3} = \frac{E_i d^3\sigma(Q)}{dp_i^3} \otimes P(E_i \rightarrow E_f) \otimes D(Q \rightarrow H_Q), \quad (1)$$

where indexes f and i refer to the final hadron (H_Q) and initial parton (Q), respectively. $\frac{E_i d^3\sigma(Q)}{dp_i^3}$ denotes the parton initial momentum distribution, calculated according to [35]. $P(E_i \rightarrow E_f)$ presents the energy loss probability based on our dynamical energy loss formalism (see below). $D(Q \rightarrow H_Q)$ stands for fragmentation function of parton into the hadron (H_Q), where for the light hadrons, D and B mesons we apply DSS [36], BCFY [37] and KLP [38] fragmentation functions, respectively.

The dynamical energy loss formalism [39–41] includes several unique features in modeling jet-medium interactions: (1) The finite size QCD medium consisting of dynamical (moving) as opposed to static scattering centers, which allows the longitudinal momentum exchange with the medium constituents. (2) The calculations within the finite temperature generalized Hard-Thermal-Loop approach [42], so that infrared divergences are naturally regulated in a highly non-trivial manner, contrary to many models which apply tree-level (vacuum-like) propagators [43–46]. (3) Both radiative [40, 41] and collisional [39] contributions are calculated within the same theoretical framework. (4) The generalization to a finite magnetic mass [47], running coupling [33] and beyond the soft-gluon approximation [48] is performed. In this paper for magnetic to electric mass ratio we assume value $\mu_M/\mu_E = 0.5$, since various non-perturbative [49, 50] approaches reported it to be in the range $0.4 - 0.6$. (5) The energy loss probability comprises also multigluon [51] and path-length [34] fluctuations. The path-length fluctuations are calculated according to the procedure presented in [52], and are provided in Ref. [53].

As outlined in Ref. [27], the analytical expression for single gluon radiation spectrum, in evolving medium, reads:

$$\begin{aligned} \frac{dN_{rad}}{dx d\tau} = & \frac{C_2(G)C_R}{\pi} \frac{1}{x} \int \frac{d^2\mathbf{q}}{\pi} \frac{d^2\mathbf{k}}{\pi} \frac{\mu_E^2(T) - \mu_M^2(T)}{[\mathbf{q}^2 + \mu_E^2(T)][\mathbf{q}^2 + \mu_M^2(T)]} T\alpha_s(ET)\alpha_s\left(\frac{\mathbf{k}^2 + \chi(T)}{x}\right) \\ & \times \left[1 - \cos\left(\frac{(\mathbf{k} + \mathbf{q})^2 + \chi(T)}{xE^+}\tau\right)\right] \frac{2(\mathbf{k} + \mathbf{q})}{(\mathbf{k} + \mathbf{q})^2 + \chi(T)} \left[\frac{\mathbf{k} + \mathbf{q}}{(\mathbf{k} + \mathbf{q})^2 + \chi(T)} - \frac{\mathbf{k}}{\mathbf{k}^2 + \chi(T)}\right], \quad (2) \end{aligned}$$

where \mathbf{k} and \mathbf{q} denote transverse momenta of radiated and exchanged gluons, respectively, $C_2(G) = 3$, $C_R = 4/3$ ($C_R = 3$) for quark (gluon) jet, while $\mu_E(T)$ and $\mu_M(T)$ are electric (Debye) and magnetic screening masses, respectively. Temperature dependent Debye mass [54] is obtained by self-consistently solving Eq. (5) from Ref. [27]. α_s is the (temperature dependent) running coupling [55], E is the initial jet energy, while $\chi(T) = M^2x^2 + m_g^2(T)$, where x is the longitudinal momentum fraction of the jet carried away by the emitted gluon, M is the mass of the quark ($M_{u,d,s} \approx \mu_E(T)/\sqrt{6}$ i.e., the thermal

mass, whereas $M_c = 1.2$ GeV and $M_b = 4.75$ GeV) or gluon jet and $m_g(T) = \mu_E(T)/\sqrt{2}$ [56] is the effective gluon mass in finite temperature QCD medium. Note that for all parameters we use standard literature values, i.e., we do not include additional fitting parameters when comparing our predictions with experimental data.

The analytical expression for the collisional energy loss per unit length in the evolving medium is given by [27]:

$$\begin{aligned} \frac{dE_{coll}}{d\tau} &= \frac{2C_R}{\pi v^2} \alpha_s(ET) \alpha_s(\mu_E^2(T)) \int_0^\infty n_{eq}(|\vec{k}|, T) d|\vec{k}| \\ &\times \left[\int_0^{|\vec{k}|/(1+v)} d|\vec{q}| \int_{-v|\vec{q}|}^{v|\vec{q}|} \omega d\omega + \int_{|\vec{k}|/(1+v)}^{|\vec{q}|_{max}} d|\vec{q}| \int_{|\vec{q}|-2|\vec{k}|}^{v|\vec{q}|} \omega d\omega \right] \\ &\times \left[|\Delta_L(q, T)|^2 \frac{(2|\vec{k}| + \omega)^2 - |\vec{q}|^2}{2} + |\Delta_T(q, T)|^2 \frac{(|\vec{q}|^2 - \omega^2)((2|\vec{k}| + \omega)^2 + |\vec{q}|^2)}{4|\vec{q}|^4} (v^2|\vec{q}|^2 - \omega^2) \right], \end{aligned} \quad (3)$$

where $n_{eq}(|\vec{k}|, T) = \frac{N}{e^{|\vec{k}|/T-1}} + \frac{N_f}{e^{|\vec{k}|/T+1}}$ is the equilibrium momentum distribution [57] comprising gluons, quarks and antiquarks ($N = 3$ and $N_f = 3$ are the number of colors and flavors, respectively). k is the 4-momentum of the incoming medium parton, v is velocity of the initial jet and $q = (\omega, \vec{q})$ is the 4-momentum of the exchanged gluon. $|\vec{q}|_{max}$ is provided in Ref. [39], while $\Delta_T(T)$ and $\Delta_L(T)$ are effective transverse and longitudinal gluon propagators given by Eqs. (3) and (4) in Ref. [27].

One of the assets of our energy loss formalism is the fact that energy loss explicitly depends on T , which makes it naturally suited for examining the QGP properties via implementation of various temperature profiles. In this paper, the temperature dependence on proper time (τ) is taken according to the ideal hydrodynamical 1+1D Bjorken expansion [26] $T(\tau) \sim \sqrt[3]{(\tau_0/\tau)}$, with thermalization time $\tau_0 = 0.6$ fm [58, 59]. The initial QGP temperature T_0 for the chosen centrality bin is determined as described in [27]. In this paper, we will concentrate on mid central 30 – 40% centrality region at 5.02 TeV $Pb + Pb$ at the LHC, which corresponds to $T_0 = 391$ MeV [27]. We however performed the extensive study on all centrality regions (as in [27]), and checked that the results/conclusions obtained here are the same irrespectively of the centrality region (results not shown for brevity). The QGP transition temperature is considered to be $T_C \approx 160$ [60].

DREENA-B framework is applied for generating predictions for two main high- p_\perp observables – R_{AA} and v_2 . R_{AA} is defined as the ratio of the quenched $A + A$ spectrum to the

$p + p$ spectrum, scaled by the number of binary collisions N_{bin} :

$$R_{AA}(p_T) = \frac{dN_{AA}/dp_T}{N_{bin}dN_{pp}/dp_T}, \quad (4)$$

while for intuitive understanding of the underlying effects we also use [53]:

$$R_{AA} \approx \frac{R_{AA}^{in} + R_{AA}^{out}}{2}, \quad (5)$$

where R_{AA}^{in} and R_{AA}^{out} denote in-plane and out-of-plane nuclear modification factors, respectively. The expression for the high- p_{\perp} elliptic flow [53, 61, 62] reads:

$$v_2 \approx \frac{1}{2} \frac{R_{AA}^{in} - R_{AA}^{out}}{R_{AA}^{in} + R_{AA}^{out}}. \quad (6)$$

III. RESULTS AND DISCUSSION

In the first part of this section we address how different initial stages (before the thermalization time τ_0) affect our predictions of high- p_{\perp} R_{AA} and v_2 . To this end, we consider the following four common cases of initial stages [23], which assume the same 1+1D Bjorken hydro temperature (T) profile [26] upon thermalization (for $\tau \geq \tau_0$), but have different T profiles before the thermalization (for $\tau < \tau_0$):

- (a) $T = 0$, the so-called *free-streaming case*, which corresponds to neglecting interactions (i.e., energy loss) before the QGP thermalization.
- (b) The *linear case*, corresponding to linearly increasing T with time from transition temperature ($T_C = 160$ MeV at $\tau_C = 0.25$ fm) to the initial temperature T_0 .
- (c) The *constant case* $T = T_0$, and
- (d) The *divergent case*, corresponding to 1+1D Bjorken expansion from $\tau = 0$.

These initial stages are depicted in Fig. 1, and it is clear that (a)-(d) case ordering corresponds to gradually increasing pre-thermal interactions. Note that we use this classification (a)-(d) consistently throughout the paper to denote initial stages (for $\tau < \tau_0$), as well as for the entire evolution. Also, note that in this part of the study, we will include experimental data for comparison with our predictions. However, to allow better visualization of our obtained numerical results, in the other two parts of the study we will omit the comparison with the data, as the error bars are large and the data remain the same.

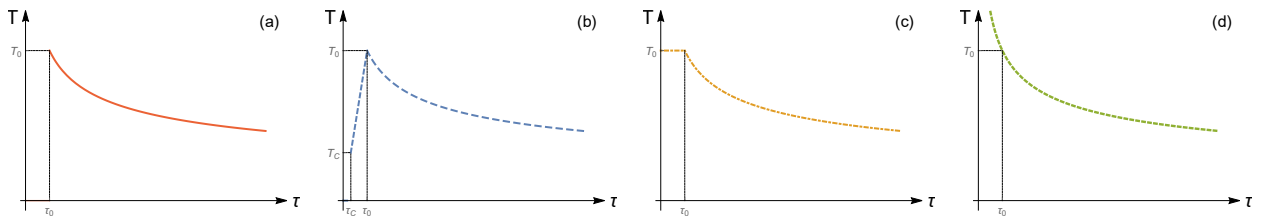


FIG. 1: Four temperature evolution profiles, which differ at the initial stages. At $\tau \geq \tau_0$, all profiles assume the same temperature dependence on the proper time (1 + 1D Bjorken [26]). At the initial stage, i.e., for $0 < \tau < \tau_0$, the temperature is considered to be: (a) equal to zero; (b) increasing linearly from T_C to T_0 between τ_C and τ_0 , otherwise zero; (c) constant and equal to T_0 ; and (d) a continuous function of τ matching the dependence for $\tau \geq \tau_0$. Note that, in each panel, T_0 has the same value at τ_0 .

Intuitively, one would expect that introducing these pre-thermal interactions would increase the energy loss compared to the commonly considered free-streaming case, and consequently lead to smaller R_{AA} . In Fig. 2 we indeed observe that R_{AA} is sensitive to the initial stages. That is, as expected, we see that the suppression progressively increases from case (a) to case (d). However, these differences are not very large, and the current errorbars at the LHC do not allow distinguishing between these scenarios, as can be seen in Fig. 2 (left).

Contrary to R_{AA} , the effect of initial stages on v_2 is intuitively less clear, as this observable non-trivially depends on the energy loss or R_{AA} s (see Eq. (6)). From Fig. 3, we surprisingly infer that v_2 is insensitive to the presumed initial stage for all types of particles (in distinction to the results obtained in [24]), so that v_2 is unable to distinguish between different initial-stage scenarios.

To quantitatively understand this unexpected observation, in Fig. 4 we show transverse momentum dependence of R_{AA}^{in} , R_{AA}^{out} and R_{AA} in $i = b, c, d$ cases relative to the baseline case (a) for charged hadrons. The conclusions for heavy particles are the same and therefore omitted. We distinguish three sets of curves, which corresponds to the ratio of R_{AA} s in a I) linear (b), II) constant (c), III) divergent (d) relative to free-streaming (a) case. Note that the free-streaming case is used as a baseline, as it corresponds to the most commonly used scenario, both in low and high- p_\perp calculations.

Each set of curves in Fig. 4 contains three lines, representing proportionality functions

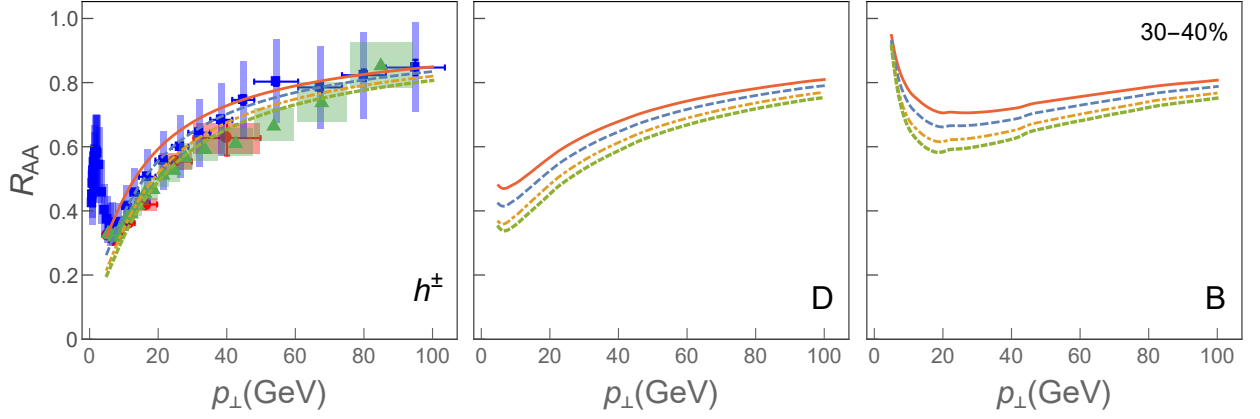


FIG. 2: R_{AA} dependence on p_{\perp} for four different initial stages depicted in Fig. 1 is shown for charged particles (*left panel*), D mesons (*central panel*) and B mesons (*right panel*). For charged hadrons, the predictions are compared with 5.02 TeV $Pb + Pb$ ALICE [7] (red circles), ATLAS [9] (green triangles) and CMS [8] (blue squares) h^{\pm} R_{AA} experimental data. In each panel, temperature profile from Fig. 1 are presented by full red curve (case a), by dashed blue curve (case b), by dot-dashed orange curve (case c) and by dotted green curve (case d). The results correspond to the centrality bin 30 – 40%, and $\mu_M/\mu_E = 0.5$.

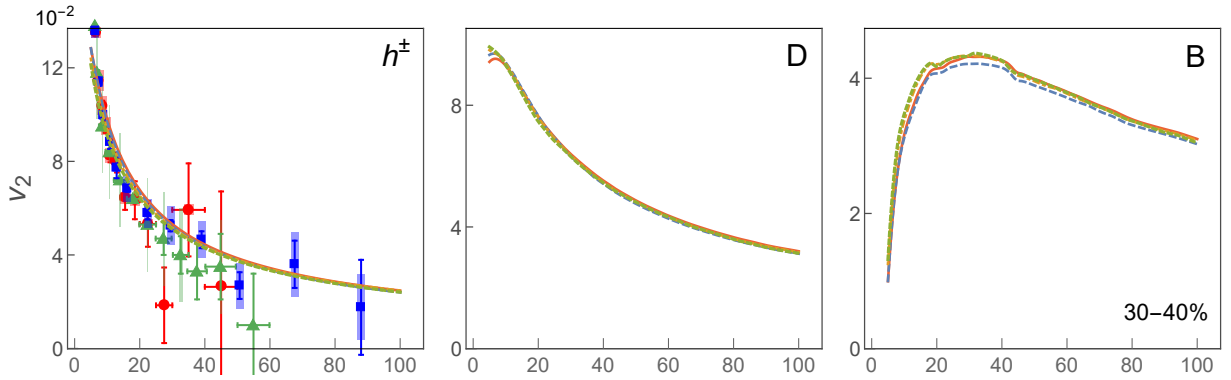


FIG. 3: v_2 dependence on p_{\perp} for four different initial stages depicted in Fig. 1. *Left, central and right panels* correspond to charged hadrons, D mesons and B mesons, respectively. For charged hadrons, the predictions are compared with 30-40% centrality 5.02 TeV $Pb + Pb$ ALICE [15] (red circles), ATLAS [17] (green triangles) and CMS [16] (blue squares) h^{\pm} v_2 experimental data. The labeling and remaining parameters are the same as in Fig. 2.

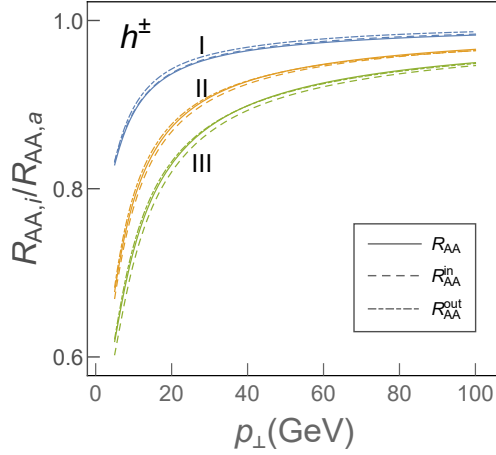


FIG. 4: Transverse momentum dependence of in-plane (dashed), out-of plane (dot-dashed) and angular averaged (full curves) R_{AA} relative to the free-streaming case for charged hadrons. Blue (upper), orange (middle) and green (lower) set of curves correspond, respectively, to I, II and III cases. The remaining parameters are the same as in Fig. 2.

$\gamma(p_{\perp})$ s, which are defined as follows:

$$\gamma_{ia}^{in} = \frac{R_{AA,i}^{in}}{R_{AA,a}^{in}}, \quad \gamma_{ia}^{out} = \frac{R_{AA,i}^{out}}{R_{AA,a}^{out}}, \quad \gamma_{ia} = \frac{R_{AA,i}}{R_{AA,a}}, \quad (7)$$

where $i = b, c, d$ denotes the corresponding cases from Fig. 1. From Fig. 4 we see that for the same i (i.e., within the same set of curves I, II or III) the proportionality functions $\gamma_{ia}(p_{\perp})$ are practically identical for the relations involving in-plane, out-of-plane and angular averaged R_{AA} s:

$$\gamma_{ia}^{in} \approx \gamma_{ia}^{out} \approx \gamma_{ia}. \quad (8)$$

Note also that $\gamma_{ia} < 1$, while γ_{ias} from distinct sets significantly differ from one another (i.e., for $i \neq j \rightarrow \gamma_{ia}(p_{\perp}) \neq \gamma_{ja}(p_{\perp})$).

Consequently, by implementing Eq. (7) in Eq. (6) and acknowledging Eq. (8), we obtain:

$$v_{2,i} \approx \frac{1}{2} \frac{\gamma_{ia}(R_{AA,a}^{in} - R_{AA,a}^{out})}{\gamma_{ia}(R_{AA,a}^{in} + R_{AA,a}^{out})} = v_{2,a}, \quad (9)$$

for any choice of $i = b, c, d$, as observed in Fig. 3. Therefore, we here showed that initial stages alone do not affect v_2 , i.e., they affect only R_{AA} . R_{AA} susceptibility to the initial stages is in a qualitative agreement with papers [27, 63, 64], where R_{AA} is shown to be only sensitive to the averaged properties of the evolving medium, i.e., average temperature (\bar{T}).

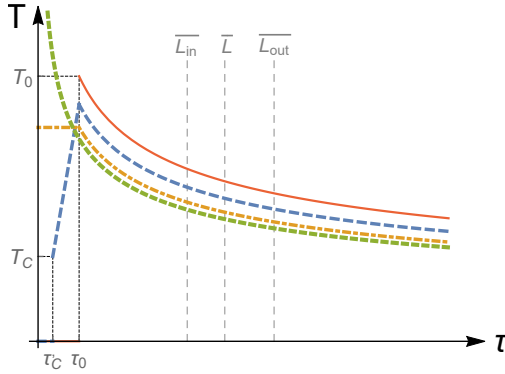


FIG. 5: Temperature dependence on the proper time in the setup with the same average temperatures. The labeling is the same as in Fig. 1, apart from the fact that initial temperatures (T_0 's) now differ in these four cases. As in Fig. 1, $T_C = 160$ MeV, $\tau_0 = 0.6$ fm and $\tau'_C = 0.27$ fm. Vertical gray dashed lines correspond to average in-medium path length (\bar{L}), and to the path lengths along in-plane (\bar{L}_{in}) and out-of-plane (\bar{L}_{out}) directions, as labeled in the figure.

Since R_{AA} is proportional to the \bar{T} , and since for all four initial-stage cases (a)-(d) the \bar{T} is different ($\bar{T}_a < \bar{T}_b < \bar{T}_c < \bar{T}_d$), it is evident that R_{AA} will be different in these cases.

The fact that R_{AA} depends on the average temperature of the medium, motivate us to further explore the case in which we modify the above temperature profiles to reproduce the same average temperature. This is equivalent to re-evaluating the initial temperatures for different cases from Fig. 1, and based on the reasoning above, it is evident that new initial temperatures should satisfy the following ordering: $T_{0,d'} < T_{0,c'} < T_{0,b'} < T_{0,a'}$. This leads to T profiles, which do not differ only at early times ($\tau < \tau_0$), but represent *different evolutions altogether*. These new evolutions, that are illustrated in Fig. 5 (which is a counterpart of Fig. 1 for the second part of this section), are denoted as (a')-(d') and referred to as "modified" T profiles ((a) \equiv (a')).

In this second T -profiles setup, we first verify from Fig. 6 that R_{AAS} in all four cases practically overlap, as expected. We next address how these modified evolution cases (a') – (d') affect v_2 . From Fig. 7 we see that v_2 is now very sensitive to the transition from free-streaming case to other modified T profiles. More accurately, for all types of particles, the lowest v_2 is observed in modified divergent case, while the highest v_2 is observed in the free-streaming case.

The observation from Fig. 7 leads to the following two questions: *i)* Why is v_2 altered

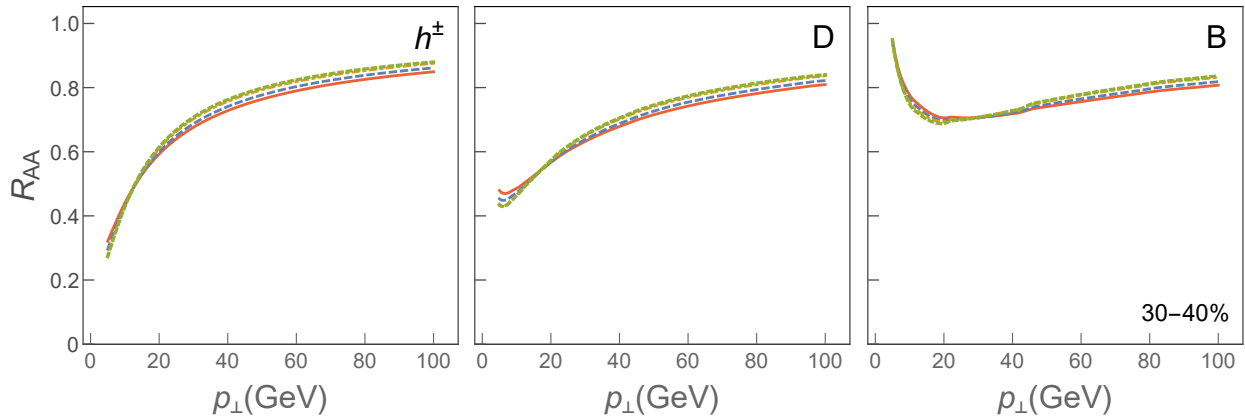


FIG. 6: R_{AA} dependence on p_{\perp} for four different medium evolutions depicted in Fig. 5. *Left, central and right panels* correspond to charged hadrons, D mesons and B mesons, respectively. In each panel, T profile corresponding to the case: (a') from Fig. 5 is presented by full red curve, (b') dashed blue curve, (c') dot-dashed orange curve and (d') dotted green curve. The results correspond to the centrality bin 30 – 40%, and $\mu_M/\mu_E = 0.5$.

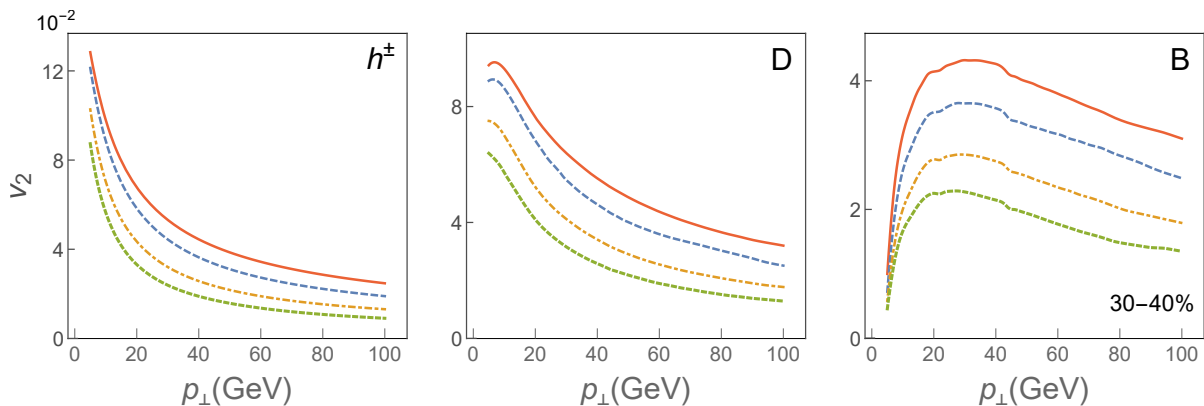


FIG. 7: v_2 dependence on p_{\perp} for four different medium evolutions depicted in Fig. 5. *Left, central and right panels* correspond to charged hadrons, D mesons and B mesons, respectively. The labeling and remaining parameters are the same as in Fig. 6.

by these modified T profiles (a') – (d')? and *ii*) Are these discrepancies a consequence of different initial stages? The answer to these questions, we first note that, within this setup, the differences between v_2 (observed in Fig. 7) are proportional to $R_{AA}^{in} - R_{AA}^{out}$, as the denominator in Eq. (6) (as a starting premise) remains practically unchanged (see Fig. 6). The transverse momentum dependence of $R_{AA}^{in} - R_{AA}^{out}$ is further shown in Fig. 8 for charged

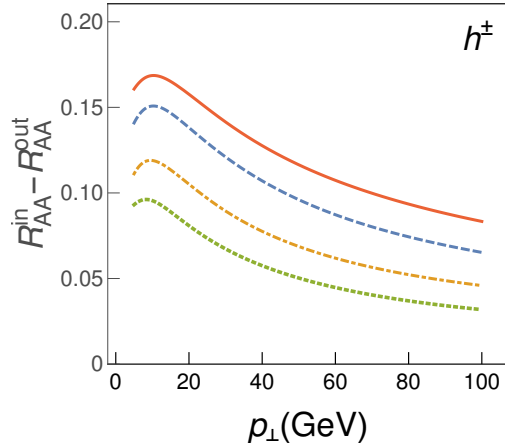


FIG. 8: $R_{AA}^{in} - R_{AA}^{out}$ dependence on p_{\perp} for charged hadrons. The labeling and remaining parameters are the same as in Fig. 6.

hadrons (as results for D and B mesons will lead to the same conclusion). We see a clear hierarchy, i.e., the largest $R_{AA}^{in} - R_{AA}^{out}$ for free-streaming, descending towards divergent case. To quantitatively understand this observation, we note that for R_{AA}^{in} , the high- p_{\perp} probes traverse, on the average, the medium up to \bar{L}_{in} , while for R_{AA}^{out} , the medium is traversed up to \bar{L}_{out} . Consequently, if we refer to Fig. 5, $R_{AA}^{in} - R_{AA}^{out}$ comes from T -profile difference in the time region between \bar{L}_{in} and \bar{L}_{out} , i.e., *upon thermalization*. Since in this region $\bar{T}_{d'} < \bar{T}_{c'} < \bar{T}_{b'} < \bar{T}_{a'}$ holds, $R_{AA}^{in} - R_{AA}^{out}$ is the largest for free-streaming case and the smallest for the divergent case, as observed in Fig. 8, and in agreement with v_2 ordering in Fig. 7. This therefore provides clarification of why $R_{AA}^{in} - R_{AA}^{out}$, and consequently v_2 , is affected by these four different QGP evolution profiles, and that this difference originates primarily from the interactions of high- p_{\perp} parton with *thermalized QGP*, and *not the initial stages*. This agrees with the first part of this section (Figs. 2 and 3), where we showed and explained insensitivity of v_2 to different initial stages. It is worth emphasizing that, contrary to the first part of this section, in the second part we tested the effects on R_{AA} and v_2 not from distinctive initial stages, but instead from four entirely different evolutions of the QCD medium (related by the same global property, i.e., average temperature).

In the final, third, part of this section we adopt a commonly used approach, in which the energy loss is fitted through change of multiplicative fitting factor in the energy loss, to reproduce the desired high- p_{\perp} R_{AA} , e.g., the one that best fits the experimental data (see e.g., [24, 30, 62, 65–67]). To this end, we use the same four T -profiles from the first

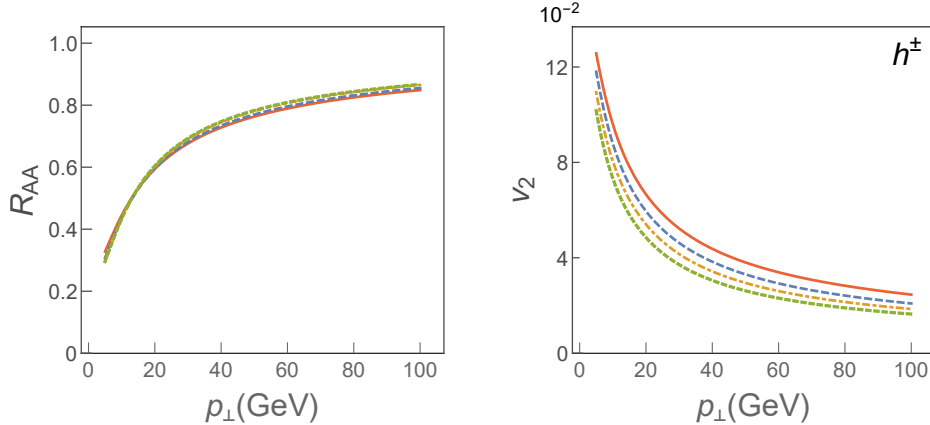


FIG. 9: R_{AA} (left panel) and v_2 (right panel) dependence on p_{\perp} for charged hadrons, when additional energy loss multiplicative factor is introduced to reproduce the free-streaming R_{AA} , in four different initial-stage cases depicted in Fig. 1. The labeling and remaining parameters are the same as in Figs. 2 and 3.

part of this section (Fig. 1), while, in our full-fledged calculations (see Sec. II) we introduce an additional multiplicative fitting factor (free parameter) C_i^{fit} , $i = b, c, d$. C_i^{fit} is then estimated for each initial-stage case as a best fit to the free-streaming R_{AA} (see Table I). Thus obtained R_{AA} s are shown in the left panel of Fig. 9 only for the representative case of h^{\pm} , as the same conclusions stand for both light and heavy flavor hadrons. From the left panel of this figure we observe practically overlapping R_{AA} s in all (a)-(d) cases, as anticipated, which is obtained by decreasing C_i^{fit} consistently from the free-streaming to the divergent case (each $C_i^{fit} \leq 1$) in order to *compensate* for the higher energy losses in the corresponding cases compared to the case (a).

T profile case	C_i^{fit}
Free-streaming case (a)	1
Linear case (b)	0.87
Constant case (c)	0.74
Divergent case (d)	0.67

TABLE I: Fitting factors values

The effect of different T -profiles from Fig. 1 after introduction of multiplicative fitting factor C_i^{fit} in full-fledged numerical procedure on v_2 is depicted on the right panel of Fig. 9,

where we see that elliptic flow in (a)-(d) cases notably differs, i.e., is the highest in the free-streaming case, while the lowest in the divergent case. Based on this observation, one could naively infer that initial stages, i.e., $\tau < \tau_0$ region (the only region in which T profiles differ), have a significant effect on v_2 , as recently observed by alternative approach [24].

However, this kind of reasoning is inconsistent with our analysis outlined in the first two parts of this section, as well as with intuitive expectation that introduction of the energy loss at the initial stage affects R_{AA} . To quantitatively understand this result, we introduce asymptotic scaling behavior [27, 53, 68]. That is, for higher p_\perp of the initial jet, and for higher centralities (where fractional energy loss is expected to be small), we can make the following estimates:

$$\Delta E/E \approx \chi \bar{T}^m \bar{L}^n, \quad (10)$$

$$R_{AA} \approx 1 - \frac{l-2}{2} \frac{\Delta E}{E} = 1 - \xi \bar{T}^m \bar{L}^n \quad (11)$$

where m, n are proportionality factors, \bar{T} is the average temperature of the QGP, \bar{L} denotes the average path length traversed by the jet, χ is a proportionality factor (that depends on p_\perp and flavor of the jet). $\xi = \frac{l-2}{2} \chi$, where l is the steepness of a power law fit to the transverse momentum distribution.

If $\Delta E/E$ is fitted by additional multiplicative factor C , the new R_{AA}^{fit} becomes

$$R_{AA,i}^{fit} \approx 1 - C_i \xi \bar{T}_i^m \bar{L}_i^n \approx 1 - C_i (1 - R_{AA,i}), \quad (12)$$

where $i = b, c, d$ and C_i ($C_i < 1, \forall i$) denotes the fitting factor, and the last part of Eq. (12) is obtained by using Eq. (11), leading to

$$C_i \approx \frac{1 - R_{AA,i}^{fit}}{1 - R_{AA,i}}, \quad (13)$$

We note that Eq. (13) is applicable to the average, in-plane and out-of-plane R_{AA} s, since the same fitting factor is consistently applied in all three cases. By imposing the condition (which quantifies the equivalence of fitted R_{AA} in (b)-(d) cases to the free-streaming case):

$$R_{AA,i}^{fit} = R_{AA,a}, \quad (14)$$

and by applying Eqs. (5)-(8) and (14), together with Eqs. (11, 12) and their in-plane and out-of-plane analogons, we obtain:

$$v_{2,i}^{fit} \approx \frac{1}{2} \frac{C_i (R_{AA,i}^{in} - R_{AA,i}^{out})}{2R_{AA,a}} = \frac{1}{2} \frac{C_i \gamma_i (R_{AA,a}^{in} - R_{AA,a}^{out})}{R_{AA,a}^{in} + R_{AA,a}^{out}} = C_i \gamma_{ia} v_{2,a}, \quad (15)$$

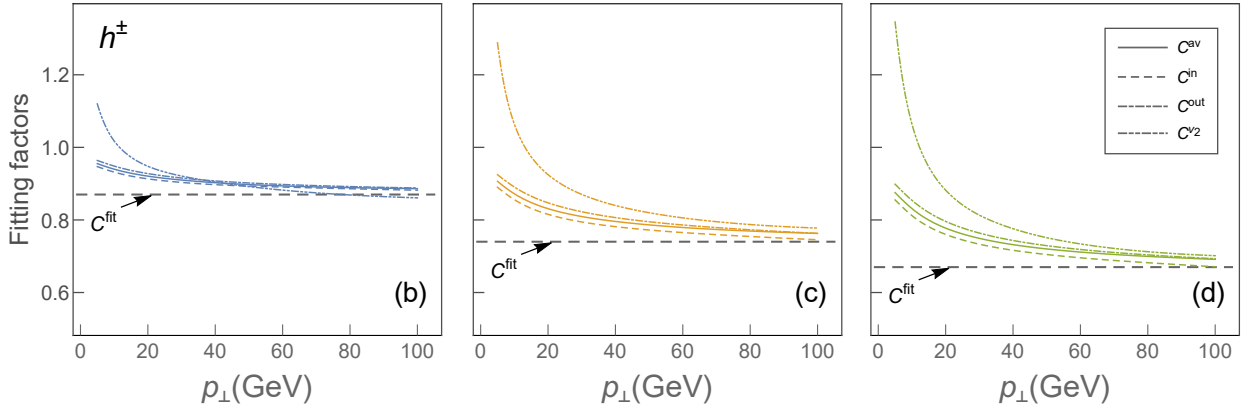


FIG. 10: Comparison of four fitting factors defined by Eq. (17) with C_i^{fit} value, obtained from full-fledged numerical procedure, in *linear* (b) (left), *constant* (c) (central) and *divergent* (d) (right panel) cases. C factors presented by full, long dashed, dot-dashed and dot-dot-dashed curves correspond to h^\pm angular averaged, in-plane, out-of-plane R_{AA} and v_2 cases, respectively. The horizontal gray dashed line presents energy loss fitted value C_i^{fit} . The results correspond to the centrality bin 30 – 40%, and $\mu_M/\mu_E = 0.5$.

which can also be written as

$$C_i \approx \frac{v_{2,i}^{fit}}{\gamma_{ia} v_{2,a}}. \quad (16)$$

From Eq. (15), we see that decrease of v_2^{fit} in (b)-(d) cases compared to (a) is a result of a fitting factor $C_i(p_\perp)$ (which is smaller than 1), as well as the proportionality functions $\gamma_i(p_\perp)$ (also smaller than 1). However, note that Eq. (15) describes asymptotic behavior at very high p_\perp , where, as mentioned earlier, γ s approach 1. Consequently, the diminishing of elliptic flow compared to the case (a) is predominantly due to a decrease of the *artificially imposed fitting factor C*. Therefore, we obtain that, contrary to [24], *initial stages are not* mainly responsible for the obtained differences (the right panel of Fig. 9) in the v_2^{fit} curves for different T profiles. Moreover, this argument, as well as the obtained inconsistency of the results in this and the first two parts of the paper, implies that application of multiple fitting procedure for each different initial stage may result in incorrect energy loss estimates and in misinterpreting the underlying physics.

To asses if this qualitative conclusion indeed holds, i.e. that v_2 succesibility observed in Fig. 9 (as well as in [24]) is indeed a consequence of a fitting factor in the energy loss, in Fig. 10 we check the consistency of Eqs. (13) and (16) with the full-fledged numerical

calculations. That is, a non-trivial consequence of Eqs. (13) and (16), is that C_i factors for the average, in-plane and out-of-plane R_{AA} s (Eq. 13) and v_2 (Eq. 16), should be the same in high- p_\perp limit, and moreover overlap with C_i^{fit} in this limit. To this end, we define the following C factors (originating from Eqs. (13, 16)):

$$\begin{aligned} C_i^{in} &= \frac{1 - R_{AA,i}^{in,fit}}{1 - R_{AA,i}^{in}}, & C_i^{out} &= \frac{1 - R_{AA,i}^{out,fit}}{1 - R_{AA,i}^{out}}, \\ C_i^{av} &= \frac{1 - R_{AA,i}^{fit}}{1 - R_{AA,i}}, & C_i^{v_2} &= \frac{1}{\gamma_{ia}} \frac{v_{2,i}^{fit}}{v_{2,a}}, \end{aligned} \quad (17)$$

and compare them with C_i^{fit} , for each separate initial-stages case, $i = b, c, d$. Note that, while expression themselves on the right-hand side of each expression in Eq. (17) are obtained in high- p_\perp limit (and consequently are expected to overlap in this limit, if our analytical estimate is valid), we calculate C_i^{fit} , and the terms on the the right-hand side of each expression in Eq. (17), through full-fledged numerical procedure. We indeed observe that, for each i and at high- p_\perp : C_i^{in} , C_i^{out} , C_i^{av} and $C_i^{v_2}$ factors are practically overlapping, and approach the value C_i^{fit} . Consequently, this highly non-trivial observation confirms that our qualitative conclusion is valid, and that v_2 susceptibility in this case is indeed a consequence of an additionally introduced fitting factor.

IV. CONCLUSIONS

Traditionally, the features of initial stages before QGP thermalization are explored through comparison of bulk medium simulations and low- p_\perp data. On the other hand, recent abundance of high- p_\perp experimental data, motivates exploiting the high- p_\perp energy loss in studying the initial stages. We here utilized state-of-the-art dynamical energy loss embedded in analytical 1+1D Bjorken medium expansion (DREENA-B framework), which allowed to tightly control the analyzed temperature profiles. In particular, we considered four temperature profiles, which are identical after, but are different before, thermalization, which correspond to four commonly considered initial-stage cases. This allowed to study the effects of different initial-stage cases on high- p_\perp R_{AA} and v_2 predictions, under highly controlled conditions, by combining full-fledged numerical results and analytical estimates used to interpret the experimental results.

We found that high- p_\perp R_{AA} is sensitive to the prethermalized stages of the medium evo-

lution, however, within the current errorbars, the sensitivity is not sufficient to distinguish between different scenarios. On the other hand, the high- p_{\perp} v_2 is unexpectedly insensitive to the initial stages. We furthermore found that previously reported sensitivity [24] of high- p_{\perp} v_2 to initial stages is mainly a consequence of the fitting procedure in which the parameters in the energy loss are adjusted to reproduce experimentally observed R_{AA} , individually for different initial-stage cases. On the other hand, if the same global property, in particular the same average temperature, is imposed to tested temperature profiles, high sensitivity of high- p_{\perp} v_2 is again obtained. This sensitivity is, however, a consequence of differences in final, rather than initial, stages. Overall, our results underscore that the simultaneous study of high- p_{\perp} R_{AA} and v_2 , with consistent/fixed energy loss parameters across the entire study and controlled temperature profiles (reflecting only the differences in the initial stages), is crucial to impose accurate constraints on the initial stages.

Acknowledgments: We thank Pasi Huovinen and Jussi Auvinen for useful discussions. This work is supported by the European Research Council, grant ERC-2016-COG: 725741, and by the Ministry of Science and Technological Development of the Republic of Serbia, under project No. ON171004 and ON173052.

-
- [1] J. C. Collins and M. J. Perry, Phys. Rev. Lett. **34**, 1353 (1975).
 - [2] G. Baym and S. A. Chin, Phys. Lett. B **62**, 241 (1976).
 - [3] M. Gyulassy and L. McLerran, Nucl. Phys. A **750**, 30 (2005).
 - [4] E. V. Shuryak, Nucl. Phys. A **750**, 64 (2005); Rev. Mod. Phys. **89**, 035001 (2017).
 - [5] B. Jacak and P. Steinberg, Phys. Today **63**, 39 (2010).
 - [6] B. Muller, J. Schukraft and B. Wyslouch, Ann. Rev. Nucl. Part. Sci. **62**, 361 (2012).
 - [7] S. Acharya *et al.* [ALICE Collaboration], JHEP **1811**, 013 (2018).
 - [8] V. Khachatryan *et al.* [CMS Collaboration], JHEP **1704**, 039 (2017).
 - [9] The ATLAS collaboration [ATLAS Collaboration], ATLAS-CONF-2017-012.
 - [10] S. Jaelani [ALICE Collaboration], Int. J. Mod. Phys. Conf. Ser. **46**, 1860018 (2018).
 - [11] J. Wang [CMS Collaboration], Nucl. Part. Phys. Proc. **289-290**, 249 (2017).
 - [12] T. W. Wang [CMS Collaboration], Nucl. Part. Phys. Proc. **289-290**, 229 (2017).
 - [13] A. Adare *et al.* [PHENIX Collaboration], Phys. Rev. Lett. **101**, 232301 (2008); Phys. Rev. C

- 87**, no. 3, 034911 (2013).
- [14] B. I. Abelev et al. [STAR Collaboration], Phys. Lett. B **655**, 104 (2007).
 - [15] S. Acharya *et al.* [ALICE Collaboration], JHEP **1807**, 103 (2018).
 - [16] A. M. Sirunyan *et al.* [CMS Collaboration], Phys. Lett. B **776**, 195 (2018).
 - [17] M. Aaboud *et al.* [ATLAS Collaboration], Eur. Phys. J. C **78**, no. 12, 997 (2018).
 - [18] S. Acharya *et al.* [ALICE Collaboration], Phys. Rev. Lett. **120**, no. 10, 102301 (2018).
 - [19] A. M. Sirunyan *et al.* [CMS Collaboration], Phys. Rev. Lett. **120**, no. 20, 202301 (2018).
 - [20] F. Gelis and B. Schenke, Ann. Rev. Nucl. Part. Sci. **66**, 73 (2016).
 - [21] G. Aad *et al.* [ATLAS Collaboration], JHEP **1311**, 183 (2013).
 - [22] H. Niemi, G. S. Denicol, H. Holopainen and P. Huovinen, Phys. Rev. C **87**, no. 5, 054901 (2013).
 - [23] J. Xu, A. Buzzatti and M. Gyulassy, JHEP **1408**, 063 (2014).
 - [24] C. Andres, N. Armesto, H. Niemi, R. Paatelainen and C. A. Salgado, arXiv:1902.03231.
 - [25] R. Katz, C. A. G. Prado, J. Noronha-Hostler, J. Noronha and A. A. P. Suaide, arXiv:1906.10768.
 - [26] J. D. Bjorken, Phys. Rev. D **27**, 140 (1983).
 - [27] D. Zigic, I. Salom, M. Djordjevic and M. Djordjevic, Phys. Lett. B **791**, 236 (2019).
 - [28] J. Xu, J. Liao and M. Gyulassy, Chin. Phys. Lett. **32**, no. 9, 092501 (2015).
 - [29] S. Shi, J. Liao and M. Gyulassy, Chin. Phys. C **42**, no. 10, 104104 (2018); Chin. Phys. C **43**, no. 4, 044101 (2019).
 - [30] J. Noronha-Hostler, B. Betz, J. Noronha and M. Gyulassy, Phys. Rev. Lett. **116**, no. 25, 252301 (2016).
 - [31] S. K. Das, F. Scardina, S. Plumari and V. Greco, Phys. Lett. B **747**, 260 (2015).
 - [32] M. Djordjevic, *et al.*, in preparation.
 - [33] M. Djordjevic and M. Djordjevic, Phys. Lett. B **734**, 286 (2014).
 - [34] S. Wicks, W. Horowitz, M. Djordjevic and M. Gyulassy, Nucl. Phys. A **784**, 426 (2007).
 - [35] Z. B. Kang, I. Vitev and H. Xing, Phys. Lett. B **718**, 482 (2012); R. Sharma, I. Vitev and B.W. Zhang, Phys. Rev. C **80**, 054902 (2009).
 - [36] D. de Florian, R. Sassot and M. Stratmann, Phys. Rev. D **75**, 114010 (2007).
 - [37] M. Cacciari, P. Nason, JHEP **0309**, 006 (2003); E. Braaten, K.-M. Cheung, S. Fleming and T. C. Yuan, Phys. Rev. D **51**, 4819 (1995).

- [38] V. G. Kartvelishvili, A.K. Likhoded, V.A. Petrov, Phys. Lett. B **78**, 615 (1978).
- [39] M. Djordjevic, Phys. Rev. C **74**, 064907 (2006).
- [40] M. Djordjevic, Phys. Rev. C **80**, 064909 (2009).
- [41] M. Djordjevic and U. Heinz, Phys. Rev. Lett. **101**, 022302 (2008).
- [42] J. I. Kapusta, *Finite-Temperature Field Theory* (Cambridge University Press, 1989).
- [43] R. Baier, Yu.L. Dokshitzer, A.H. Mueller, S. Peigne and D. Schiff, Nucl. Phys. B **483** (1997) 291; Nucl. Phys. B **484**, 265 (1997).
- [44] N. Armesto, C.A. Salgado and U.A. Wiedemann, Phys. Rev. D **69**, 114003 (2004).
- [45] M. Gyulassy, P. Levai and I. Vitev, Nucl. Phys. B **594**, 371 (2001).
- [46] X.N. Wang and X.F. Guo, Nucl. Phys. A **696**, 788 (2001).
- [47] M. Djordjevic, Phys. Lett. B **709**, 229 (2012).
- [48] B. Blagojevic, M. Djordjevic and M. Djordjevic, Phys. Rev. C **99**, no. 2, 024901 (2019).
- [49] Yu. Maezawa *et al.* [WHOT-QCD Collaboration], Phys. Rev. D **81**, 091501 (2010).
- [50] A. Nakamura, T. Saito and S. Sakai, Phys. Rev. D **69**, 014506 (2004).
- [51] M. Gyulassy, P. Levai and I. Vitev, Phys. Lett. B **538**, 282 (2002).
- [52] A. Dainese, Eur. Phys. J. C **33**, 495 (2004).
- [53] D. Zigic, I. Salom, J. Auvinen, M. Djordjevic and M. Djordjevic, J. Phys. G **46**, 085101 (2019).
- [54] A. Peshier, hep-ph/0601119 (2006).
- [55] R. Field, Applications of Perturbative QCD, Perseus Books, Cambridge, Massachusetts (1995).
- [56] M. Djordjevic and M. Gyulassy, Phys. Rev. C **68**, 034914 (2003).
- [57] E. Braaten and M. H. Thoma, Phys. Rev. D **44**, 1298 (1991).
- [58] P. F. Kolb and U. W. Heinz, "Hydrodynamic description of ultrarelativistic heavy ion collisions," in Quark-Gluon Plasma 3, eds. R. C. Hwa and X.-N. Wang (World Scientific, Singapore, 2004), p. 634. [nucl-th/0305084].
- [59] J. E. Bernhard, J. S. Moreland and S. A. Bass, Nucl. Phys. A **967**, 293 (2017).
- [60] A. Bazavov *et al.* [HotQCD Collaboration], Phys. Rev. D **90**, 094503 (2014).
- [61] P. Christiansen, K. Tywoniuk and V. Viskovic, Phys. Rev. C **89**, no. 3, 034912 (2014).
- [62] B. Betz and M. Gyulassy, JHEP **1408**, 090 (2014) Erratum: [JHEP **1410**, 043 (2014)].
- [63] T. Renk, Phys. Rev. C **85**, 044903 (2012).
- [64] D. Molnar and D. Sun, Nucl. Phys. A **932**, 140 (2014); **910-911**, 486 (2013).

- [65] B. Betz, M. Gyulassy, M. Luzum, J. Noronha, J. Noronha-Hostler, I. Portillo and C. Ratti, Phys. Rev. C **95**, no. 4, 044901 (2017).
- [66] C. A. G. Prado, J. Noronha-Hostler, R. Katz, A. A. P. Suaide, J. Noronha, M. G. Munhoz and M. R. Cosentino, Phys. Rev. C **96**, no. 6, 064903 (2017).
- [67] S. Cao *et al.* [JETSCAPE Collaboration], Phys. Rev. C **96**, no. 2, 024909 (2017).
- [68] M. Djordjevic, D. Zigic, M. Djordjevic and J. Auvinen, Phys. Rev. C **99**, no.6, 061902 (2019).